Effective thermal conductivity of two-phase functionally graded particulate composites

H. M. Yin, G. H. Paulino,[a)] and W. G. Buttlar
Department of Civil and Environmental Engineering, University of Illinois at Urbana-Champaign, Newmark Laboratory, 205 North Mathews Avenue, Illinois 61801

L. Z. Sun
Department of Civil and Environmental Engineering and Center for Computer-Aided Design, The University of Iowa, Iowa City, Iowa 52242

A multiscale modeling method is proposed to derive effective thermal conductivity in two-phase graded particulate composites. In the particle-matrix zone, a graded representative volume element is constructed to represent the random microstructure at the neighborhood of a material point. At the steady state, the particle's averaged heat flux is solved by integrating the pairwise thermal interactions from all other particles. The homogenized heat flux and temperature gradient are further derived, through which the effective thermal conductivity of the graded medium is calculated. In the transition zone, a transition function is introduced to make the homogenized thermal fields continuous and differentiable. By means of temperature boundary conditions, the temperature profile in the gradation direction is solved. When the material gradient is zero, the proposed model can also predict the effective thermal conductivity of uniform composites with the particle interactions. Parametric analyses and comparisons with other models and available experimental data are presented to demonstrate the capability of the proposed method. © *2005 American Institute of Physics*. [DOI: 10.1063/1.2039998]

I. INTRODUCTION

Graded materials are characterized by spatially varied microstructures of constituent phases and gradual variation of effective material properties. These microstructures are not only found in natural materials such as bamboo and wood,[1] but also occur in some civil engineering materials and constructed facilities.[1,2] For instance, asphalt pavements are typically constructed in layers, where material gradients such as density (vertically graded air void concentration) are built into the pavement through roller compaction. Additionally, when a layer is compacted onto a dissimilar substrate layer, a macroscopically sized interface zone arises due to the intermingling of coarse aggregates, which are approximately 5–25 mm in diameter, and the binder materials. In addition, above the groundwater table, the moisture content varies in the vertical direction, which also creates material property gradients. Finally, the temperature field in pavements also varies, particularly with depth from the surface, causing the viscoelastic asphalt surfacing materials to exhibit significant physical property gradients (creep compliance, fracture toughness, etc.). Since thermal cracking of pavements is a devastating pavement distress that can occur in cold and/or rapidly changing climates, the ability to accurately predict thermal fields within a pavement as a function of time is essential in the selection of materials to avoid this problem.[3]

Materials with graded microstructures, or *functionally graded materials* (FGMs), have been successfully manufactured for various applications.[1,2,4] In ceramic/metal FGMs, a continuous trade-off of fracture toughness and high thermal conductivity of metals is made with ceramic hardness and low thermal conductivity. In heat and impact protection applications, the material multifunctionality consists of the ability to provide structural support by virtue of the metallic portions of FGMs, and the simultaneous ability of the same material system to provide the required thermal or impact resistance by virtue of the ceramic portions of FGMs. The effective thermal properties in the gradation direction are essential for designing these materials and predicting their service behaviors.[5]

Effective thermal conductivity of heterogeneous materials has been extensively investigated in theoretical, numerical, and experimental methods[6–9] considering different particle shapes, sizes, and volume fractions. While FGMs have been designed and fabricated by diverse methods to achieve the gradual material transition in the gradation direction, very limited analytical investigations are available to tackle the spatial variation of microstructure.[10] *Conventional composite models* such as Maxwell-Garnett's model[11] and the self-consistent method[12] have been directly applied to estimate the effective thermal conductivity of FGMs. Because they were originally developed for homogeneous mixtures with constant particle concentration, those models are not able to capture the material gradient nature of FGMs. Furthermore, no direct interactions between particles are taken into consideration.[10]

The purpose of this work is to investigate the effective thermal conductivity and temperature profile in FGMs with particle interactions and particle distributions. We place an FGM between two parallel platens and apply constant tem-

---

[a)]Electronic mail: paulino@uiuc.edu
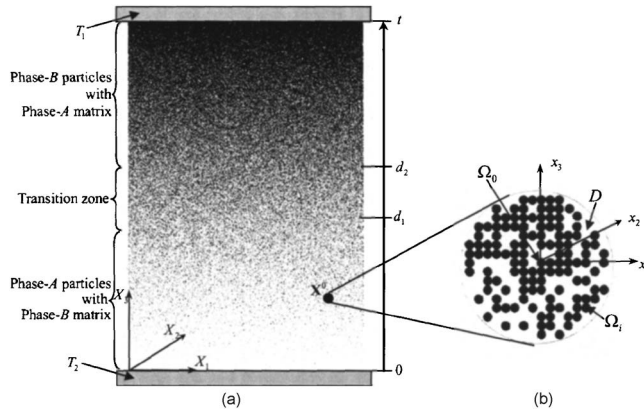
FIG. 1. Schematic of the modeled FGM plate, placed between two platens with fixed temperatures T_1 and T_2: (a) the macrosystem and (b) illustration of the RVE in the neighborhood of the material at point $\mathbf{X}^0$.

peratures T_1 and T_2 on the two platens, respectively. The FGM, illustrated in Fig. 1(a), microscopically contains a particle-matrix zone with dispersed particles filled in continuous matrix, followed by a skeletal transition zone in which the particle and matrix phases cannot be well defined because the two phases are interpenetrated into each other as a connected network. The transition zone is further followed by another particle-matrix zone with interchanged phases of particle and matrix.[13] For simplicity, both phases are assumed to be isotropic solids, and in the particle-matrix zones particles are assumed to be identical spheres fully bonded to the matrix in the absence of interfacial thermal resistance.[14]

A formulation is proposed to derive the averaged heat flux field of both phases in the particle-matrix zone, and a transition function is constructed to solve the averaged fields in the transition zone. From the relation between the effective flux and temperature gradient, the effective thermal-conductivity distribution in the gradation direction is determined. In the course of derivation, a microscopic representative volume element (RVE),[13,15] as seen in Fig. 1(b), is proposed to statistically represent the microstructure in the neighborhood of a material point in the particle-matrix zone, and the equivalent inclusion method[6,16] is employed to derive the averaged heat flux of particles in the RVE.

When we only consider one particle-matrix zone, the present model can be used to predict the behavior of graded materials where the particle and matrix phases do not become interchanged. If the gradient of the volume fraction distribution is zero, the FGM is reduced to a standard composite containing uniformly dispersed particles and an explicit simplified solution of the effective thermal conductivity is provided. Mathematically, the effective thermal conductivity is a quantity analogous to effective electric conductivity, dielectric permittivity, magnetic permeability, or water permeability in a linear static state, so this method can be easily extended to those problems as well.[5,17]

The remainder of this paper is organized as follows. Section II briefly reviews the equivalent inclusion method and formulates the pairwise particle interaction. Section III employs the pairwise interaction in the microscale thermal analysis of FGMs and solves the relation of averaged heat fluxes of two phases for a material point in the particle-

matrix zone. Section IV calculates the effective thermal conductivity and temperature profile in the gradation direction of FGMs. Section V presents some parametric studies and further compares the proposed model with other models and available experimental data.

II. PAIRWISE PARTICLE INTERACTION

To investigate the disturbed elastic field for a single ellipsoidal inhomogeneity filled in the infinite domain under a uniform far-field loading, Eshelby[16] proposed the equivalent inclusion method, in which the inhomogeneity is transferred to the same material as the matrix but an eigenstrain is introduced in the inclusion domain to simulate the material mismatch. Hatta and Taya[6] extended Eshelby's method to heat conduction problems. Since then, the equivalent inclusion method has been widely employed in modeling the effective thermal conductivity of heterogeneous composites.[18,19]

Consider a single spherical particle with the radius a embedded in an infinite, homogeneous matrix under a uniform heat flux field $\mathbf{q}^0$. Because the particle and the matrix have different thermal conductivities, denoted as k_1 and k_0, respectively, the heat flux in the neighborhood of the particle will be distorted. Based on the equivalent inclusion method, the material mismatch can be simulated by introducing a distributed doublet[6] with the strength $\mathbf{q}^*(\mathbf{x})$ on the particle domain Ω, so the total domain is treated as a homogeneous material with thermal conductivity k_0 and subjected to a uniform flux $\mathbf{q}^0$ and a doublet on the particle domain. Then the local temperature gradient $\nabla T(\mathbf{x})$ in the equivalent homogeneous domain comes from two sources: the applied uniform flux $\mathbf{q}^0$ and the disturbed flux $\mathbf{q}'$ due to $\mathbf{q}^*(\mathbf{x})$, namely,

$$\nabla T(\mathbf{x}) = -\frac{1}{k_0}[\mathbf{q}^0 + \mathbf{q}'(\mathbf{x})], \tag{1}$$

where $\mathbf{q}'(\mathbf{x})$ can be solved by the Green's-function technique[20] as

$$\mathbf{q}'(\mathbf{x}) = \int_\Omega \mathbf{\Gamma}(\mathbf{x} - \mathbf{x}') \cdot \mathbf{q}^*(\mathbf{x}')d\mathbf{x}', \tag{2}$$

in which $\mathbf{\Gamma}(\mathbf{x} - \mathbf{x}')$ is the so-called modified Green's function[20] for the scalar potential written as

$$\mathbf{\Gamma}(\mathbf{x} - \mathbf{x}') = \frac{1}{4\pi} \nabla \otimes \nabla \varphi, \tag{3}$$

with $\varphi = 1/|\mathbf{x} - \mathbf{x}'|$. It represents the response flux at an arbitrary point $\mathbf{x}$ due to the unit source flux at a certain point $\mathbf{x}'$. Here, the source flux is a distributed doublet on the particle domain Ω, so the disturbed flux at any point $\mathbf{x}$ is written as an integral in Eq. (2).

In the real configuration with the particle being different from the matrix, the Fourier law of heat conduction reads

$$\mathbf{q}(\mathbf{x}) = \begin{cases} -k_1 \nabla T(\mathbf{x}), & \mathbf{x} \in \Omega \\ -k_0 \nabla T(\mathbf{x}), & \mathbf{x} \notin \Omega. \end{cases} \tag{4}$$

From the flux equivalent condition, the flux in the real particle should be equal to that in the equivalent inclusion, so we obtain

$$-k_1 \nabla T(\mathbf{x}) = -k_0 \nabla T(\mathbf{x}) + \mathbf{q}^*(\mathbf{x}), \quad \mathbf{x} \in \Omega. \tag{5}$$

It is noted that, in the equivalent inclusion, the flux includes the temperature-induced flux and the prescribed doublet $\mathbf{q}^*$. Using Eqs. (4) and (5), we can solve

$$\mathbf{q}^*(\mathbf{x}) = \frac{k_1 - k_0}{k_1} \mathbf{q}(\mathbf{x}). \tag{6}$$

Combining Eqs. (1), (2), and (6), we can derive that the doublet and heat flux field in the particle domain are still uniform as

$$\mathbf{q}^*(\mathbf{x}) = 3\beta \mathbf{q}^0, \quad \mathbf{x} \in \Omega, \tag{7}$$

and

$$\mathbf{q}(\mathbf{x}) = \alpha \mathbf{q}^0, \quad \mathbf{x} \in \Omega, \tag{8}$$

with

$$\alpha = \frac{3k_1}{k_1 + 2k_0}, \quad \beta = \frac{k_1 - k_0}{k_1 + 2k_0}. \tag{9}$$

Here

$$\int_\Omega \boldsymbol{\Gamma}(\mathbf{x} - \mathbf{x}') d\mathbf{x}' = -\boldsymbol{\delta}/3 \quad \text{for } \mathbf{x} \in \Omega \tag{10}$$

is used with $\boldsymbol{\delta}$ being the second-rank unit tensor or the Kronecker delta tensor.

Let us further add another identical particle into the domain. Then, the disturbed flux comes from the two particle source domains as

$$\mathbf{q}'(\mathbf{x}) = \int_\Omega \boldsymbol{\Gamma}(\mathbf{x} - \mathbf{x}') \cdot \mathbf{q}^*(\mathbf{x}') d\mathbf{x}'$$
$$+ \int_{\Omega'} \boldsymbol{\Gamma}(\mathbf{x} - \mathbf{x}') \cdot \mathbf{q}^*(\mathbf{x}') d\mathbf{x}', \tag{11}$$

in which Ω' represents the new particle domain. The distributed doublet and total heat flux in the particle domains will no longer be uniform due to the particle interaction when the particle center-to-center distance is not too large. Expanding the distributed doublet and heat flux of particles in a polynomial form of the local coordinates,[18,21,22] we can also solve Eqs. (1), (6), and (11) for the heat flux field. After a lengthy but straightforward derivation, the averaged heat flux in each spherical particle domain is calculated as[22]

$$\bar{\mathbf{q}} = \alpha(1 - \beta\rho^3 + \beta^2\rho^6)\mathbf{q}^0 + 3\alpha(\beta\rho^3 + \beta^2\rho^6)\mathbf{n} \otimes \mathbf{n} \cdot \mathbf{q}^0$$
$$+ O(\rho^8), \tag{12}$$

where

$$\mathbf{n} = (\mathbf{x}_1 - \mathbf{x}_2)/|\mathbf{x}_1 - \mathbf{x}_2|, \quad \rho = a/|\mathbf{x}_1 - \mathbf{x}_2|, \tag{13}$$

with $\mathbf{x}_1$ and $\mathbf{x}_2$ being the centers of two particles, respectively. Comparing Eqs. (8) and (12), we can find that the additional particle provides an interaction on the averaged field of the first particle as[22]

$$\mathbf{d}(\mathbf{x}_1, \mathbf{x}_2) \triangleq \bar{\mathbf{q}} - \alpha\mathbf{q}^0$$
$$= \alpha\beta\rho^3[(-\boldsymbol{\delta} + 3\mathbf{n} \otimes \mathbf{n})$$
$$+ \beta\rho^3(\boldsymbol{\delta} + 3\mathbf{n} \otimes \mathbf{n})] \cdot \mathbf{q}^0 + O(\rho^8), \tag{14}$$

which is the so-called *pairwise thermal interaction* between particles.

III. MICROSCALE THERMAL ANALYSIS OF FGMS

Consider a typical FGM microstructure [Fig. 1(a)] containing two phases A and B with isotropic thermal conductivities k_A and k_B, respectively. The global coordinate system of the FGM is denoted by (X_1, X_2, X_3) with X_3 being the continuous gradation direction. The overall grading thickness of the FGM is t. Three material zones exist in the gradation direction: Zone I $(0 \leq X_3 \leq d_1)$ including phase A particles with phase B matrix, zone III $(d_2 \leq X_3 \leq t)$ including phase B particles with phase A matrix, and the transition (or intermediate) zone II $(d_1 \leq X_3 \leq d_2)$. We place this FGM between two parallel platens and apply temperatures T_2 and T_1 at the lower and upper platens $(T_2 \neq T_1)$, respectively. In each particle-matrix zone, particles are assumed to be identical and be fully bonded to the matrix. A steady-state problem, without heat sources in the FGM, is considered.

For any macroscopic material point $\mathbf{X}^0$ [Fig. 1(a)] in the range of $0 \leq X_3 \leq d_1$ (zone I), the corresponding microstructural RVE [Fig. 1(b)] contains a number of microparticles of phase A embedded in a continuous matrix of phase B so that the overall volume fraction of particle phase A and the its gradient should be consistent with the macroscopic counterparts $\phi(X_3^0)$ and $d\phi/dX_3|_{X_3=X_3^0}$. The microscopic coordinate system $(x_1, x_2, \text{and } x_3)$ is constructed with the origin corresponding to $\mathbf{X}^0$. All microparticles are assumed to be spherical with identical radius $a (a \ll t)$ for straightforward formulation. As seen in Fig. 1(b), the whole RVE domain is denoted as D and the ith microparticle $(i = 1, 2, 3, \ldots, \infty)$ domain is denoted as Ω_i centered at $\mathbf{x}^i$. For the ease of formulation, a particle centered at the origin is assumed and denoted as Ω_0.

Due to the particle interactions in the RVE, the local heat flux field in each particle is nonuniform for many particles embedded in the matrix. However, we can write the averaged heat flux of the central particle in two parts: the material-mismatch interaction between the central particle and the matrix in Eq. (8) and the pairwise interaction between the central particle and all other particles in Eq. (14) as

$$\langle \mathbf{q} \rangle^A(0) = \alpha\langle \mathbf{q} \rangle^B(0) + \sum_{i=1}^{\infty} \mathbf{d}(\mathbf{0}, \mathbf{x}^i), \tag{15}$$

where the angular brackets $\langle \cdot \rangle^A$ and $\langle \cdot \rangle^B$ denote the volume averages over phase A and phase B in the $X_1 - X_2$ layer, respectively.

Because all the particles are statistically distributed in a random way, the probability of particle distribution can be introduced to statistically demonstrate the particle interaction effect. Therefore, the pairwise interaction [i.e., the second term of the right-hand side of Eq. (15)] can be further integrated over all possible particle positions as[13]

$$\langle \mathbf{d} \rangle(0) = \int_D \mathbf{d}(0,\mathbf{x}) P(\mathbf{x}|0) d\mathbf{x}, \tag{16}$$

where $P(\mathbf{x}|0)$ is the *conditional number density function* used to find a particle centered at $\mathbf{x}$ when the first particle is located at 0. For statistically homogeneous composite materials containing randomly distributed spherical particles with the volume fraction ϕ, the particle probability density function is frequently proposed as[23]

$$P(\mathbf{x}|0) = \frac{3\phi g(x)}{4\pi a^3}, \tag{17}$$

where x denotes the distance from $\mathbf{x}$ to 0, or $|\mathbf{x}|$. The term $3\phi/(4\pi a^3)$, in fact, indicates the total number of particles per unit volume. The other term $g(x)$ is the radial distribution function of particles proposed by Percus and Yevick[24] to estimate the particle nonuniformity effect in the radial direction.

For the FGM considered, since the microparticles in RVE are distributed in a continuously increasing manner in the gradation direction, the particle density function is proposed as

$$P(\mathbf{x}|0) = \frac{3g(x)}{4\pi a^3}[\phi(X_3^0) + e^{-x/\delta}\phi_{,3}(X_3^0)x_3]. \tag{18}$$

Here the expression enclosed by the square brackets is constructed on the basis that the averaged volume fraction of particle in the RVE is $\phi(X_3^0)$, the gradient of particle volume fraction is $\phi_{,3}(X_3^0)$, and in the far field the particle concentration must not be beyond the range of zero to the maximum particle concentration. Thus, an exponential function is introduced to attenuate the gradation term exponentially. The parameter δ, which controls the attenuating rate, will be determined under the conditions that the maximum volume fraction of particles in the RVE should not be greater than the maximum volume fraction in particle-matrix zone and the minimum one should not be less than zero. Thus, it is calculated by the following condition:

$$\delta = \frac{e}{\phi_{,3}(X_3^0)} \min(\phi, \phi^c - \phi), \tag{19}$$

where ϕ^c denotes the maximum volume fraction in the particle-matrix zone. Since the particle interaction is quickly attenuated with the increment of the distance between particles, those particles in the neighboring domain of the central particle should contribute the majority part for the averaged flux of the central particle.

In the chosen RVE, due to the graded microstructure, the matrix's averaged heat flux changes in the gradation direction. It should be differentiable and bounded over the RVE. To analytically integrate Eq. (16), the averaged heat flux $\langle \mathbf{q} \rangle^B(x_3)$ is approximated by the Taylor expansion. Because the thermal interaction between the central particle and the particles far away from it is negligible, only the particles in the close neighborhood of the central particle may have noticeable interaction on the central particle. As a first-order approximation, we truncate the Taylor expansion of $\langle \mathbf{q} \rangle^B(x_3)$ to linear term in terms of x_3 so that Eq. (16) can be analytically integrated and rewritten as

$$\langle \mathbf{d} \rangle(0) = \phi(X_3^0)\mathbf{D}(0) \cdot \langle \mathbf{q} \rangle^B(0) + \phi_{,3}(X_3^0)\mathbf{F}(0) \cdot \langle \mathbf{q} \rangle_{,3}^B(0), \tag{20}$$

where

$$\mathbf{D} = \int_D \frac{3g(x)}{4\pi x^3}\alpha\beta[(-\boldsymbol{\delta} + 3\mathbf{n} \otimes \mathbf{n}) \\ + \beta\rho^3(\boldsymbol{\delta} + 3\mathbf{n} \otimes \mathbf{n})]d\mathbf{x},$$

$$\mathbf{F} = \int_D e^{-x/\delta}\frac{3g(x)}{4\pi x}\alpha\beta[(-\boldsymbol{\delta} + 3\mathbf{n} \otimes \mathbf{n}) + \beta\rho^3(\boldsymbol{\delta} + 3\mathbf{n} \otimes \mathbf{n})]n_3^2 d\mathbf{x}. \tag{21}$$

The above two integration terms $\mathbf{D}$ and $\mathbf{F}$ can be further simplified. The volume element $d\mathbf{x} = dx_1 dx_2 dx_3$ can be expressed as $d\mathbf{x} = x^2 d\omega dx$, where $x \triangleq |\mathbf{x}|$ and $d\omega$ is the surface element on the unit sphere Σ centered at the origin of the coordinates. The integrals in Eq. (21) along the surface of Σ can be explicitly derived and then only one-dimensional numerical integration in terms of x should be calculated as

$$D_{ij} = \int_{2a}^{\infty} \frac{g(x)}{x} 6\alpha\beta^2\rho^3\delta_{ij}dx,$$

$$F_{ij} = \int_{2a}^{\infty} 3g(x)xe^{(x/\delta)}\alpha\beta\left[\left(-\frac{\delta_{ij}}{3} + \frac{\delta_{ij} + 2\delta_{i3}\delta_{j3}}{5}\right) \\ + \beta\rho^3\left(\frac{\delta_{ij}}{3} + \frac{\delta_{ij} + 2\delta_{i3}\delta_{j3}}{5}\right)\right]dx. \tag{22}$$

Substituting Eq. (20) into (15) and recognizing that the origin of the local coordinates in the RVE corresponds to the global coordinate point $\mathbf{X}^0$ of FGMs, we can obtain the particle's averaged flux in terms of the arbitrary material point X_3 as

$$\langle \mathbf{q} \rangle^A(X_3) = \alpha\langle \mathbf{q} \rangle^B(X_3) + \phi(X_3)\mathbf{D}(X_3) \cdot \langle \mathbf{q} \rangle^B(X_3) \\ + \phi_{,3}(X_3)\mathbf{F}(X_3) \cdot \langle \mathbf{q} \rangle_{,3}^B(X_3). \tag{23}$$

Interchanging the matrix and particle phases, we can similarly derive the relation between the averaged fluxes of two phases in the range of $d_2 \le X_3 \le t$ (zone III).

IV. EFFECTIVE THERMAL BEHAVIOR OF FGMS

Due to the temperature difference between the upper and lower boundaries, a steady-state heat flux is induced in the gradation direction of the FGM. The particle distribution in each X_1-X_2 layer is statistically homogeneous. Thus, based on the energy balance, the averaged heat flux in each X_1-X_2 layer at the steady state should be the same, which is denoted as $\mathbf{q}^0$ with $q_1^0 = q_2^0 = 0$. The averaged heat flux and temperature

gradient in the X_1-X_2 layer are defined as the volume average of the flux and temperature gradient on the two phases, and are expressed as

$$\langle \mathbf{q} \rangle (X_3) = \mathbf{q}^0 = \phi(X_3)\langle \mathbf{q} \rangle^A(X_3) + [1 - \phi(X_3)]\langle \mathbf{q} \rangle^B(X_3) \tag{24}$$

and

$$\langle \nabla T \rangle (X_3) = -\phi(X_3)\langle \mathbf{q} \rangle^A(X_3)/k_A - [1 - \phi(X_3)] \\ \times \langle \mathbf{q} \rangle^B(X_3)/k_B. \tag{25}$$

From the relation between the averaged heat flux and temperature gradient, we can calculate effective thermal conductivity in the X_1-X_2 layer.

With the combination of Eqs. (23) and (24), the particle's averaged flux $\langle \mathbf{q} \rangle^A(X_3)$ and the matrix's averaged flux $\langle \mathbf{q} \rangle^B(X_3)$ in the FGM gradation direction X_3 can be solved in terms of the averaged flux $\mathbf{q}^0$. Since Eq. (23) is a set of ordinary differential equations, we also need the appropriate boundary conditions. In the particle-matrix zone with $0 \leq X_3 \leq d_1$, the boundary at $X_3=0$ corresponds to the 100% matrix material [i.e., $\phi(0)=0$]. The corresponding boundary conditions can be proposed as

$$\langle \mathbf{q} \rangle^B(0) = \mathbf{q}^0. \tag{26}$$

Therefore, the averaged flux field in both phases can be numerically solved on the basis of standard backward Eulerian method. Similarly, in the other particle-matrix zone with the range of $d_2 \leq X_3 \leq t$ (zone III), we can also calculate the averaged flux fields by interchanging the matrix and particle phases. It is noted that, for those FGMs whose particle volume fraction does not start from 0%, the boundary condition in Eq. (26) is no longer valid. The modified boundary condition of $\langle \mathbf{q} \rangle^B(0)$ can be still obtained in terms of $\mathbf{q}^0$ with the aid of the uniform composite model as seen in Eq. (34), which will be discussed later in this section.

For the transition zone II ($d_1 < X_3 < d_2$), the particle and matrix phases cannot be well defined because the two phases may be interpenetrated into each other as a connected network. As a consequence, the averaged flux fields of both phases cannot explicitly be determined through the above framework. Following Yin *et al.*,[13] a phenomenological transition function is introduced as

$$f(X_3) = \left[1 - 2\frac{\phi(X_3) - \phi(d_1)}{\phi(d_1) - \phi(d_2)}\right]\left[\frac{\phi(X_3) - \phi(d_2)}{\phi(d_1) - \phi(d_2)}\right]^2, \tag{27}$$

so that the averaged flux of each phase (A or B) in the transition zone II can be approximated as the combination of the solutions for two particle-matrix zones. Namely,

$$\langle \mathbf{q} \rangle^{A \text{ or } B}_{\text{zone-II}}(X_3) = f(X_3)\langle \mathbf{q} \rangle^{A \text{ or } B}_{\text{zone-I}}(X_3) + [1 - f(X_3)] \\ \times \langle \mathbf{q} \rangle^{A \text{ or } B}_{\text{zone-III}}(X_3). \tag{28}$$

Once we obtain the averaged flux of each phase in the FGM, the overall averaged heat flux and temperature gradient at each X_1-X_2 layer can be further obtained from Eqs. (24) and (25). Then we can solve the effective thermal conductivity at that layer as

$$\bar{k}(X_3) = -q_3^0/\langle T_{,3} \rangle (X_3). \tag{29}$$

It is noted that the proposed transition function satisfies the requirement that the effective FGM thermal conductivity should be bounded, continuous, and differentiable in the gradation direction.

The temperature distribution in the gradation direction is essential for investigation of thermoelastic behavior of FGMs.[12,25] Once the effective thermal conductivity is solved, the temperature gradient in the gradation direction of FGMs is related to the heat flux $\mathbf{q}^0$ under the Fourier law as Eq. (29). The heat flux $\mathbf{q}^0$ essentially depends on the boundary conditions on the upper and lower surfaces. Obviously, the two platens in Fig. 1(a) provide constant temperature boundary conditions as

$$T|_{X_3=0} = T_2, \quad T|_{X_3=t} = T_1. \tag{30}$$

Integrating the temperature gradient in the gradation direction in Eq. (29), we can obtain the following equation:

$$\int_0^t \frac{q_3^0}{\bar{k}(\xi)}d\xi = T_2 - T_1. \tag{31}$$

Since $\vec{k}(\xi)$ has been solved, the heat flux $\mathbf{q}^0$ can be calculated with $q_1^0=q_2^0=0$ from the above equation, and then the temperature distribution in the gradation direction is written as

$$T(X_3) = T_2 - \int_0^{X_3} \frac{q_3^0}{\bar{k}(\xi)}d\xi. \tag{32}$$

It is noted that although these formulations are developed for FGMs, if the gradient of the microstructure is zero or the volume fraction of particles is constant in all directions, this model is still applicable to the uniform composites with randomly dispersed particles. Then Eq. (23) is reduced into

$$\langle \mathbf{q} \rangle^A = \alpha \langle \mathbf{q} \rangle^B + \phi \mathbf{D} \cdot \langle \mathbf{q} \rangle^B. \tag{33}$$

Combining Eqs. (24) with (33), we can directly solve the averaged fluxes of both phases in terms of $\mathbf{q}^0$ as

$$\langle \mathbf{q} \rangle^B = [\phi(\alpha \boldsymbol{\delta} + \phi \mathbf{D}) + (1 - \phi)\boldsymbol{\delta}]^{-1} \cdot \mathbf{q}^0,$$

$$\langle \mathbf{q} \rangle^A = [\phi + (1 - \phi)(\alpha \boldsymbol{\delta} + \phi \mathbf{D})^{-1}]^{-1} \cdot \mathbf{q}^0. \tag{34}$$

Therefore, we can easily solve the temperature gradient through Eq. (25), from which we conclude that the temperature linearly changes between the two platens. Using an approximation of the particle radial distribution function $g(x) = 1$ in Eq. (21), we can explicitly solve for $\mathbf{D}$ and then write the effective thermal conductivity as[22]

$$\bar{k} = k_B \frac{\phi\alpha[1 + (\phi/4)\beta^2] + (1 - \phi)}{\phi(k_B/k_A)\alpha[1 + (\phi/4)\beta^2] + (1 - \phi)}. \tag{35}$$

Here we assume phase A being particles and phase B being matrix. From Eqs. (14) and (21), we know that the terms including β describe the pairwise interactions between particles. When dropping all terms related to β, Eq. (35) is reduced to Maxwell-Garnett's model.[11]
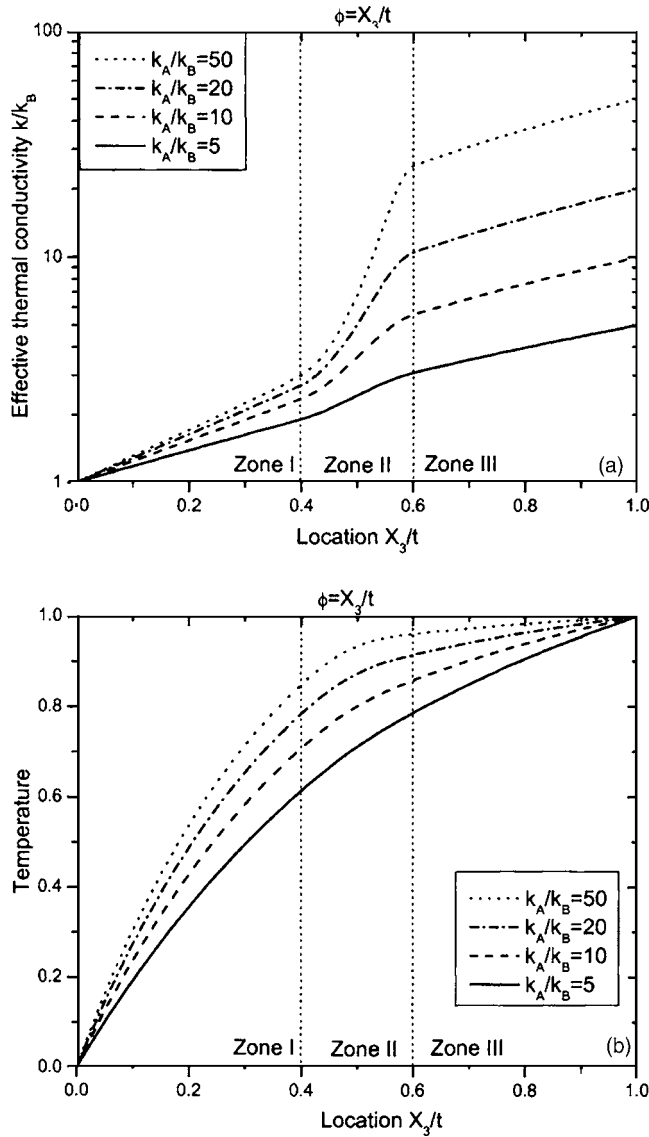
FIG. 2. Effect of thermal-conductivity contrast ratio on (a) the effective thermal conductivity and (b) temperature distributions in the FGM.

FIG. 3. (a) Effective thermal-conductivity distribution and (b) temperature distribution in an alumina/nickel FGM between the proposed model simulation. The curves denote the proposed prediction; the symbols denote the parallel model (Ref. 27).

V. NUMERICAL RESULTS AND DISCUSSION

In Fig. 1(a), the temperatures of the upper and lower boundaries of the FGM are prescribed through two constant-temperature platens with temperatures T_1 and T_2, respectively. For simplicity, we set dimensionless temperatures $T_1 = 1$ and $T_2 = 0$. A steady-state heat flux field is induced in the FGM. Obviously, the temperature distribution depends on the thermal property of each phase and microstructure of the FGM. Figure 2 shows the effect of phase thermal-conductivity contrast ratio. Specifically, the effective thermal conductivity [Fig. 2(a)] in the FGM gradation direction increases as the volume fraction of phase A increases, ranging from zone I (phase A as particle phase) to zone II (transition zone) to zone III (phase A as matrix phase). A continuous and differentiable jump is observed in the transition zone II when the phase-conductivity contrast ratio is large. Unless otherwise stated, the lower and upper bounds d_1 and d_2 are conveniently selected where the corresponding volume fractions are 40% and 60%, respectively, which follows Bao and

Cai's suggestion.[26] Here linear volume fraction distribution is considered. The temperature distributions are illustrated in Fig. 2(b). In zone I, the temperature increases faster than that in zone III due to the smaller effective thermal conductivity. It is noted that if phase A is the same as phase B, the FGM is reduced to a homogeneous material, then the temperature field should be linearly distributed in the gradation direction. The larger the thermal conductivity of phase A, the higher the temperature field in the FGM except at the upper and lower boundaries. Because the temperature field has higher-order continuity than the thermal conductivity, the curves for the temperature distribution are quite smooth in the entire FGM.

Changing the phase volume fraction distribution also affects the thermal responses of FGMs. Awaji *et al.*[27] studied temperature distributions in the alumina/nickel FGMs with different volume fraction distributions using the parallel model. Figure 3 illustrates the effective thermal conductivity

and temperature distribution in the gradation direction of FGMs and compares the proposed predictions with those of the parallel model. The FGMs include alumina as phase *A* and nickel as phase *B* with the thermal conductivities as k_A =28.2 W/mK and k_B=90.1 W/mK,[27] respectively. The transition zone is bounded as $\phi(d_1)$=40% and $\phi(d_2)$=60%. It is shown from Fig. 3 that the effective thermal conductivity of the alumina/nickel FGMs is in the range of k_B-k_A as expected. However, at a given location, the effective conductivities are strongly dependent on the phase volume fraction distribution, suggesting that the overall thermal behavior can be tailored through phase distribution pattern for desired FGM material design. It is noted that the parallel model offers an upper bound for the effective thermal conductivity of composites, and thus provides a higher prediction compared to the proposed model. Although the effective thermal conductivities for different volume fraction distributions are quite different, both models show that the temperature distributions in the gradation direction are still similar when the thermal conductivities of both phases are not overly different. However, the heat flow through the FGMs should be much different for the three cases of volume fraction distributions.

Conventional composite models (e.g., Maxwell-Garnett's model[11]) do not directly take into account the local particle interactions and gradient effects of phase volume fractions. On the contrary, our proposed model adopts the pairwise local interaction between particles and includes the effect of material gradient in the multiscale framework. Therefore, the proposed prediction depends not only on the phase volume fraction, but on the gradient of volume fraction as well. More specifically, the second term of the right-hand side in Eq. (23) denotes the pairwise interaction contribution while the third term represents the gradient effect. Disregarding these two interaction terms, we find that the proposed model recovers the standard Maxwell-Garnett's model. Equation (35) simplifies the interaction contribution but does not include the gradient effect. To clearly show the effect of the particle interactions, we consider a FGM only including one particle-matrix zone with the phase thermal-conductivity contrast ratio k_A/k_B=100 and a hyperbolic tangent volume fraction distribution function[28] $\phi(X_3)$ =0.5 tanh(βX_3) with the homogeneity parameter selected as β=1. With the increase of X_3, the gradient of volume fraction is reduced and thus the top end of the material is gradually transformed to a uniform composite with volume fraction equal to 0.5. Although the thickness of this FGM can be unlimited, Fig. 4 shows the effective thermal-conductivity distribution in the range of $0 \leqslant X_3 \leqslant 2$. When the volume fraction is small, the three methods provide the similar predictions due to small particle interactions. However, for a large volume fraction, Maxwell-Garnett's model provides the smallest prediction; whereas the FGM model produces the highest one. Because the simplified model in Eq. (35) does not consider the nonuniformity effect of particle distribution due to the central particle, it gives a lower estimate than the FGM model. When the precision is not highly emphasized, Eq. (35) can be used as a substitute for the FGM model due to the simplicity and explicitness.
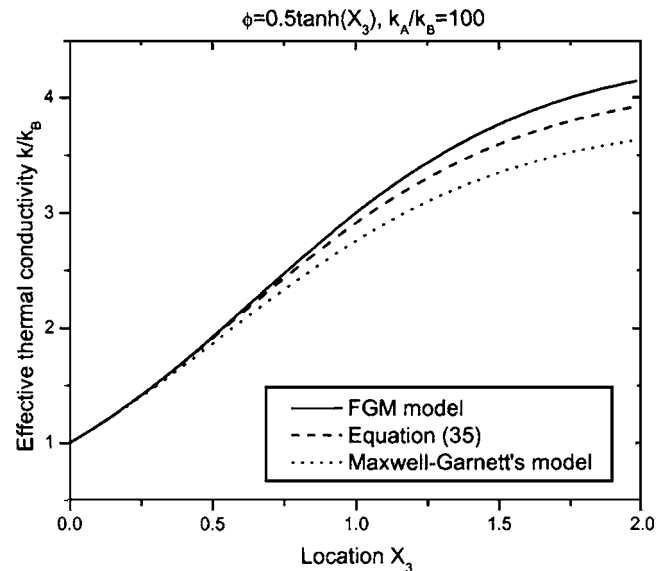
FIG. 4. Effect of the particle interactions on the effective FGM conductivity distribution.

Numerical simulations of the proposed model are also compared with available experimental data to demonstrate the validity of the model. Figure 5 shows the effective thermal-conductivity distribution in a ZrO_2/NiCoCrAlY FGM with the linear volume fraction distribution. In the experiments of Khor and co-workers,[29,30] the thermal conductivity and density of NiCoCrAlY are measured as 4.3 W/mK and 7.324 g/cm^3, respectively. The thermal conductivity and density of ZrO_2 directly from FGM are obtained as 2 W/mK and 6 g/cm^3.[31] Setting the transition zone as the volume fraction of ZrO_2 from ϕ=40% to 60%, we obtain the effective thermal-conductivity distribution varying with the weight fraction of ZrO_2 in Fig. 5. Due to the difficulty in the remelting of ZrO_2 powders during spraying, there are some gaps or pores formed between ZrO_2 particles when the vol-
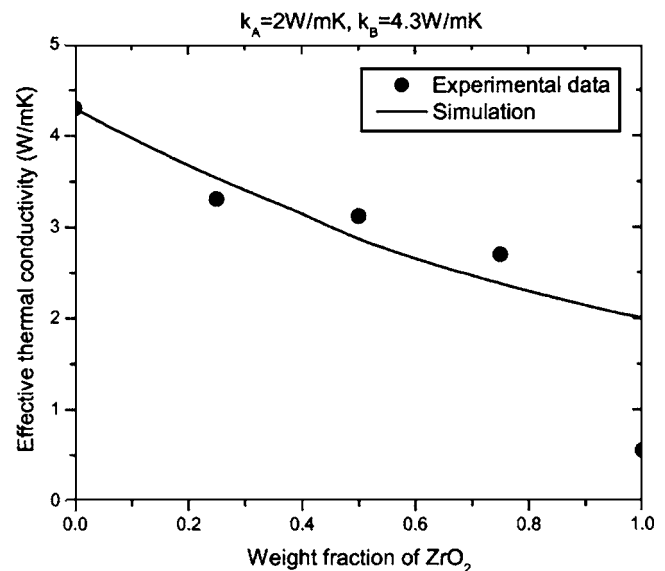
FIG. 5. Comparisons of effective thermal-conductivity distribution in a ZrO_2/NiCoCrAlY FGM between the proposed model simulation and experimental data (Ref. 30).
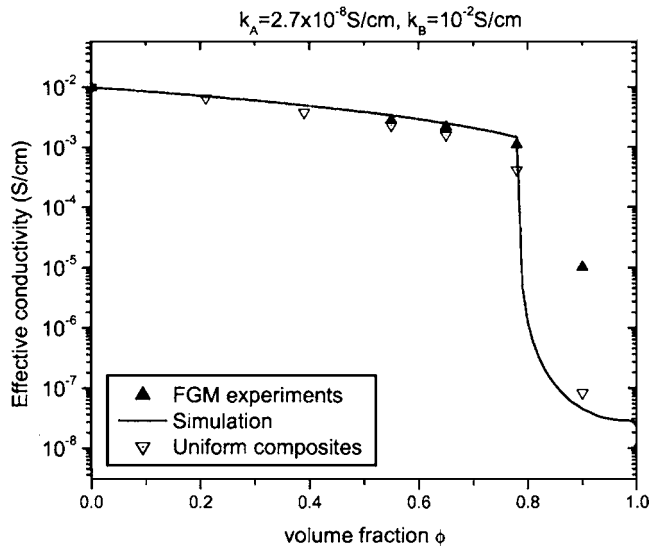
FIG. 6. Comparisons of effective conductivity distribution in an Al_2O_3/Y-TZP FGM between the proposed model simulation and experimental data (Ref. 32).

FIG. 7. Comparisons of effective thermal conductivity of uniform composites between the proposed model and experimental data (Ref. 33).

ume fraction of ZrO_2 is large.[30] Thus, we can see that the measured effective thermal conductivity for 100% ZrO_2 is much lower than 2 W/mK. Otherwise, the proposed model provides a good agreement with the experimental data.

In a linear static state, effective electric conductivity, dielectric permittivity, magnetic permeability, and water permeability can be solved mathematically analogous to effective thermal conductivity, so the proposed model can also be employed in those problems for graded materials. Sanchez-Herencia *et al.*[32] measured the electric conductivity of an alumina (Al_2O_3) and yttria tetragonal zirconia polycrystalline (Y-TZP) FGM and compared with the corresponding uniform composites. Figure 6 shows the comparison of effective conductivity distribution between the proposed prediction and experimental data. The electric conductivities of Al_2O_3 and Y-TZP are 2.7×10^{-8} and 1.0×10^{-2} S/cm, respectively. In the simulation, linear volume fraction distribution is employed and the transition zone is bounded as $\phi(d_1) = 78\%$ and $\phi(d_2) = 95\%$. It is noted that here the percolation limit is as high as 78%. When the volume fraction is less than the percolation limit, the good conductor Y-TZP is the matrix so electric flux is readily transmitted; but when the volume fraction is larger than the percolation limit, Y-TZP becomes the discrete particles so the effective electric conductivity rapidly decreases and approaches the conductivity of Al_2O_3.

When the gradient of volume fraction distribution is vanished, the proposed FGM model can also be used to predict the effective thermal conductivity of uniform composites. Wong and Bollampally[33] measured the effective thermal conductivities of epoxy-based composites containing three kinds of fillers as silica, alumina, or silica-coated aluminum nitride (SCAN). The thermal conductivities are given as $k_{epoxy} = 0.195$, $k_{silica} = 1.5$, $k_{alumina} = 36$, and $k_{SCAN} = 220$ W/mK, respectively. In Fig. 7, we see that the proposed model is in close agreement with the experimental data of silica-filled epoxy, whereas it provides much lower estimates for the two
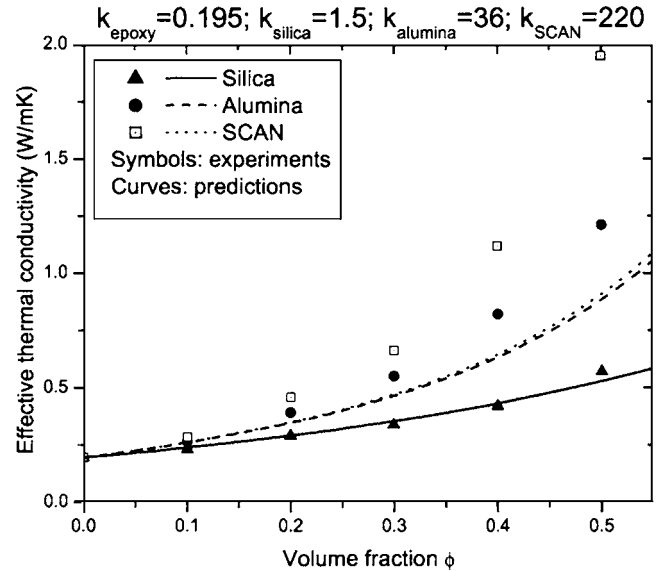
other composites. As seen in the experiments, silica particles are perfectly spherical but the two other fillers have very irregular shapes. Because the proposed model is developed for spherical particles, it produces a reasonably good prediction for the silica composites. In addition, for the proposed model, when the conductivity of particles is much higher than that of matrix, further increasing particle's conductivity will not change the effective conductivity very much because those good conductors are isolated by the matrix. Thus we can see that the curves for alumina and SCAN are very close though their thermal conductivities are much different. However, in the experiments because particles are irregular, they can readily connect with each other in the composite and form some "channels" through which heat flux can easily pass. Thus, the effective conductivity much increases along with the particle's conductivity. Because the mixtures with a high volume fraction of nonspherical particles are very common in engineering materials, an extension of this work to rigorously consider the effect of the particle shape and connected microstructure is underway.

VI. CONCLUSIONS

Effective thermal conductivity of graded materials is crucial for the calculation of the temperature profile and investigation of the thermomechanical behavior of these materials. This paper studies the effective thermal conductivity and temperature profile in FGMs considering the pairwise particle interactions and particle distributions. First, the pairwise particle thermal interaction is defined by the equivalent inclusion method. Then placing an FGM between two parallel platens with different constant temperatures, we investigate the heat flux distribution in the FGM at the steady state. In the microscale, a graded RVE is constructed to simulate the graded microstructure. Considering pairwise particle interactions in the RVE, a formulation is proposed to derive the averaged heat flux fields of both phases in the particle-matrix zone and a transition function is constructed to solve the

averaged fields in the transition zone. From the relation between the effective flux and temperature gradient in the gradation direction, the effective thermal-conductivity distribution is solved.

When we only consider one particle-matrix zone, this model can be used to predict general graded materials whose particle and matrix phases are not interchanged. If the gradient of the volume fraction distribution is zero, the FGM is reduced to a composite containing uniformly dispersed particles and an explicit approximation solution of the effective thermal conductivity is provided. By dropping the interaction term, this model recovers Maxwell-Garnett's model. This method can be easily extended to solve effective electric conductivity, dielectric permittivity, magnetic permeability, and water permeability of graded composites in a linear static state. Parametric analyses and comparisons with other models and available experiments are conducted to further validate the proposed model.

ACKNOWLEDGMENT

[1] Y. Miyamoto, W. A. Kaysser, B. H. Rabin, A. Kawasaki, and R. G. Ford, *Functionally Graded Materials: Design, Processing and Applications* (Kluwer Academic, Dordrecht, 1999).

[2] G. H. Paulino, Z. H. Jin, and R. H. Dodds, in *Comprehensive Structural Integrity*, edited by B. Karihaloo and W. G. Knauss (Elsevier Science, Amsterdam, 2003), Vol. 2, Chap. 13, pp. 607–644.

[3] R. Roque, D. R. Hiltunnen, and W. G. Buttlar, Asph. Paving Technol. **64**, 718 (1995).

[4] S. Suresh and A. Mortensen, *Fundamentals of Functionally Graded Materials* (IOM Communications Ltd., London, 1998).

[5] A. Sutradhar and G. H. Paulino, Int. J. Numer. Methods Eng. **60**, 2203 (2004).

[6] H. Hatta and M. Taya, Int. J. Eng. Sci. **24**, 1159 (1986).

[7] M. Ostoja-Starzewski and J. Schulte, Phys. Rev. B **54**, 278 (1996).

[8] A. Bhattacharya, V. V. Calmidi, and R. K. Mahajan, Int. J. Heat Mass Transfer **45**, 1017 (2002).

[9] J. Q. Tarn and Y. M. Wang, Int. J. Heat Mass Transfer **47**, 5741 (2004).

[10] J. Aboudi, M.-J. Pindera, and S. M. Arnold, Composites, Part B **30**, 777 (1999).

[11] J. C. M. Garnett, Philos. Trans. R. Soc. London, Ser. A **203**, 385 (1904).

[12] T. Reiter and G. J. Dvorak, J. Mech. Phys. Solids **46**, 1655 (1998).

[13] H. M. Yin, L. Z. Sun, and G. H. Paulino, Acta Mater. **52**, 3535 (2004).

[14] A. G. Every, Y. Tzou, D. P. H. Hasselman, and R. Raj, Acta Metall. Mater. **40**, 123 (1992).

[15] S. Nemat-Nasser and M. Hori, *Micromechanics: Overall Properties of Heterogeneous Materials*, 2nd ed. (North-Holland, Amsterdam, 1999).

[16] J. D. Eshelby, Proc. R. Soc. London, Ser. A **A241**, 376 (1957).

[17] A. Sutradhar and G. H. Paulino, Comput. Methods Appl. Mech. Eng. **193**, 4511 (2004).

[18] T. Chen and S. H. Yang, Acta Mech. **111**, 41 (1995).

[19] S. Y. Lu and H. C. Lin, J. Appl. Phys. **79**, 6761 (1996).

[20] E. Kröner, *Micromechanics and Inhomogeneity*, edited by G. L. Weng, M. Taya, and H. Abé (Springer, New York, 1990), pp. 197–211.

[21] Z. A. Moschovisdis and T. Mura, ASME J. Appl. Mech. **42**, 847 (1975).

[22] H. M. Yin and L. Z. Sun, Phys. Rev. B **72**, 054409 (2005).

[23] J. W. Ju and T. M. Chen, Acta Mech. **103**, 123 (1994).

[24] J. K. Percus and G. J. Yevick, Phys. Rev. **110**, 1 (1958).

[25] V. A. Buryachenko and F. G. Rammerstorfer, Arch. Appl. Mech. **71**, 249 (2001).

[26] G. Bao and H. Cai, Acta Mater. **45**, 1055 (1997).

[27] H. Awaji, H. Takenaka, S. Honda, and T. Nishikawa, JSME Int. J., Ser. A **44**, 37 (2001).

[28] J. H. Kim and G. H. Paulino, Int. J. Numer. Methods Eng. **58**, 1457 (2003).

[29] Y. W. Gu, K. A. Khor, Y. Q. Fu, and Y. Wang, Surf. Coat. Technol. **96**, 305 (1997).

[30] K. A. Khor and Y. W. Gu, Thin Solid Films **372**, 104 (2000).

[31] The thermal conductivity and density of Y_2O_3 stabilized ZrO_2 are 2 W/mK and 6 g/cm^3 as seen at http://www.accuratus.com/zirc.html

[32] A. J. Sanchez-Herencia, R. Moreno, and J. R. Jurado, J. Eur. Ceram. Soc. **20**, 1611 (2000).

[33] C. P. Wong and R. S. Bollampally, J. Appl. Polym. Sci. **74**, 3396 (1999).